

Structural evolution and electronic properties of pure and semiconductor atom doped in clusters: In_n^- , In_nSi^- , and In_nGe^- ($n = 3-16$)

Kai Wang | Lin Miao | Zezhao Jia | Runyu Wang | Guangjia Yin |
Xiaodong Zhu | Ramiro Moro | Lei Ma 

Tianjin International Center for Nanoparticles and Nanosystems, Tianjin University, Tianjin, China

Correspondence

Lei Ma, Tianjin International Center for Nanoparticles and Nanosystems, Tianjin University, 92 Weijin Road, Nankai District, Tianjin 300072, China.
Email: lei.ma@tju.edu.cn

Funding information

National Natural Science Foundation of China, Grant/Award Number: 11774255; the National Key R&D Program of China, Grant/Award Number: 2020YFC2004602

Abstract

The bonding and electronic properties of In_n^- , In_nSi^- , and In_nGe^- ($n = 3-16$) clusters have been computationally investigated. An intensive global search for the ground-state structures of these clusters were conducted using the genetic algorithm coupled with density functional theory (DFT). The ground-state structures of these clusters have been identified through the comparison between simulated photoelectron spectra (PES) of the found lowest-energy isomers and the experimentally measured ones. Doping semiconductor atom (Si or Ge) can significantly change the structures of the In clusters in most sizes, and the dopant prefers to be surrounded by In atoms. There are three structural motifs for In_nX^- ($\text{X} = \text{Si}, \text{Ge}, n = 3-16$), and the transition occurs at sizes $n = 5$ and 13 . All In_nSi^- and In_nGe^- share the same configurations and similar electronic properties except for $n = 8$. Among all above studied clusters, In_{13}^- stands out with the largest vertical detachment energy (VDE), HOMO-LUMO gap, (E_b) and second order energy difference Δ^2E due to its closed electronic shell of $(1S)^2(1P)^6(1D)^{10}(2S)^2(1F)^{14}(2P)^6$. Similarly, the neutral In_{12}X ($\text{X} = \text{Si}, \text{Ge}$) clusters are also identified as superatoms but with electronic configuration of $(1S)^2(1P)^6(2S)^2(1D)^{10}(1F)^{14}(2P)^6$.

KEYWORDS

density functional theory, global search, indium clusters, structural evolution, superatoms

1 | INTRODUCTION

Clusters of the group-IIIa elements aluminum, gallium, and indium have attracted much attention¹⁻⁹ due to their free-electron-like but much complex electronic configurations. For example, measurements of ionization potentials of Al_n and In_n clusters ($6 < n < 80$) show their electronic shell closing effects, but they still significantly deviate from the shell model.² Polarizability measurements of Al_{1-60} clusters also show much complicated electronic properties for $n < 40$.³ In order to explore the electronic properties of these clusters, great effort has been devoted to

investigate their geometric and electronic structures. PES measurements of Al_n^- ($n = 2-162$)⁶⁻⁸ clusters were first reported showing their electronic structures. Then, structures of pure and doped Al clusters with different sizes ($\text{Al}_{2-15}^{0,\pm 1}$,¹⁰ $\text{Al}_{13-34}^{0,\pm 1}$,¹¹ Al_{2-40} ,¹² Al_{2-65} ,¹³ Al_{35-70}^- ,¹⁴ Al_{1-6}N ,¹⁵ $\text{Al}_{2-17}\text{Mg}$,¹⁶ Al_nP_n [$n = 2-9$],¹⁷ $\text{Al}_{1-15}\text{Pt}^{18}$) were predicted theoretically. The latest study has determined the ground-state structures of Al_{13-75} cluster anions by high-precision PES measurements combined with DFT calculations.¹⁹ The results show that their electronic structures highly couple with their geometric structures, and that only for size $n = 66$ the density of states can be well explained by spherical jellium model.¹⁹ For Ga clusters, there have also been numerous theoretical works on revealing their structural and electronic properties, including

Kai Wang and Lin Miao contributed equally to this work.

Ga₁₋₆,²⁰ Ga₂₋₈,²¹ Ga₁₋₅Al,²² Ga₁₋₁₀Ti^{0,+1},²³ Ga₁₃M (M = Li, Na, K, and Rb),²⁴ Ga₂₋₂₆,²⁵ Ga₁₃₋₃₇^{0,+1},²⁶ and Ga₂₀₋₄₀.²⁷ However, so far, there are only a few studies on the pure and doped In clusters, such as In₂₋₁₅^{0,+1},²⁸ In₂₋₁₆,²⁹ In₁₋₁₃N,³⁰ In₁₋₁₀N₂,³¹ and In₁₋₁₅P₁₋₁₅^{0,-},³² and most of the confirmed structures are merely limited in the range of $n = 2-16$. Therefore, we conducted a global search for the ground-state structures of In_{*n*}⁻ and In_{*n*}X⁻ (X = Si, Ge, $n = 3-16$), and compared the simulated PES of the found ground-state structures with the reported experimental data,³³ furthermore, their electronic properties were investigated.

2 | COMPUTATIONAL METHODS

Obtaining reliable cluster structures is prerequisite for unveiling their properties. Therefore, global searches for the ground state structures of In_{*n*}⁻, In_{*n*}Si⁻, and In_{*n*}Ge⁻ ($n = 3-16$) clusters were conducted by using a homemade genetic algorithm³⁴⁻³⁶ incorporated with the quantum chemistry software ORCA³⁷ for energy calculations. The built-in def2-SVP basis set^{38,39} and the generalized gradient approximation (GGA) with the BP86^{40,41} functional were adopted for DFT calculations. In order to reach higher accuracy, the def2-TZVP basis set^{38,39} was employed to further optimize the top 10-20 candidate isomers, and then the diffuse def2-TZVP basis set (def2-TZVPD)⁴² was employed to obtain more accurate energy and simulated PES. When we conduct the geometry optimization and energy calculations, the Resolution of the Identity Approximation (RIA)⁴³ was adopted for a better computing efficiency. From the test of other six functionals in the Supporting information S1, BP86 is proved to be the most suitable one for the electronic properties of In_{*n*}⁻, In_{*n*}Si⁻, and In_{*n*}Ge⁻ clusters.

The simulated PES of the Lowest-Lying Isomers (LLIs) were generated according to the generalized Koopmans' theorem⁴⁴ which were used as criteria to evaluate the correctness of the found lowest-energy structures of In_{*n*}⁻, In_{*n*}Si⁻, and In_{*n*}Ge⁻ ($n = 3-16$) by comparing to the previously measured PES by others.³³ The stability of In_{*n*}⁻ and In_{*n*}X⁻ (X = Si, Ge) clusters was evaluated by the binding energy (E_b) defined by Equations (1) and (2):

$$E_b(\text{In}_n^-) = [(n-1)E(\text{In}) + E(\text{In}^-) - E(\text{In}_n^-)]/n \quad (1)$$

$$E_b(\text{In}_n\text{X}^-) = [nE(\text{In}) + E(\text{X}^-) - E(\text{In}_n\text{X}^-)]/(n+1) \quad (2)$$

where $E(\text{In}_n^-)$ and $E(\text{In}_n\text{X}^-)$ are the energies of the anionic In_{*n*}⁻ and In_{*n*}X⁻ clusters, $E(\text{In})$, $E(\text{In}^-)$, and $E(\text{X}^-)$ are the energies of an individual In atom, In anion and X anion, respectively. The second order differences in energy (Δ^2E) of In_{*n*}⁻, and In_{*n*}X⁻ (X = Si, Ge) were calculated using Equations (3) and (4):

$$\Delta^2E(\text{In}_n) = E(\text{In}_{n-1}) + E(\text{In}_{n+1}) - 2E(\text{In}_n) \quad (3)$$

$$\Delta^2E(\text{In}_n\text{X}^-) = E(\text{In}_{n-1}\text{X}^-) + E(\text{In}_{n+1}\text{X}^-) - 2E(\text{In}_n\text{X}^-) \quad (4)$$

The clusters structures were rendered by using the software visual molecular dynamics (VMD).⁴⁵ Bonding properties have been

investigated, including average bond length and Wiberg bond order, which were extracted using the Multiwfn 3.8 (dev) software⁴⁶ from the output of ORCA.

3 | RESULTS AND DISCUSSIONS

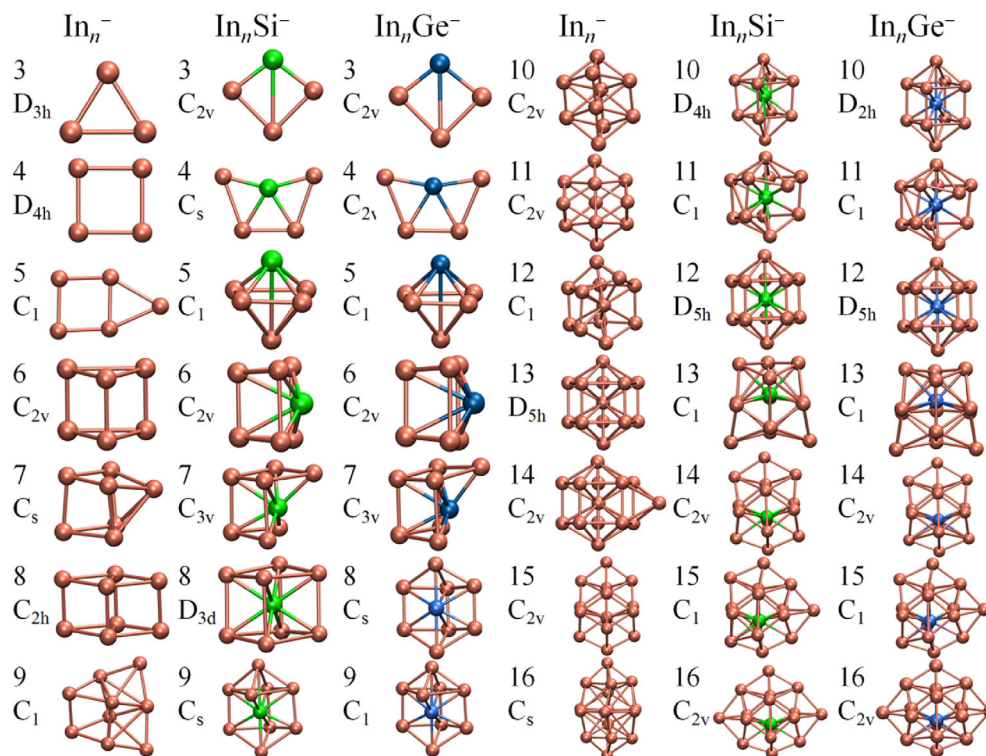
3.1 | Structures of the lowest-lying In_{*n*}⁻, In_{*n*}Si⁻, and In_{*n*}Ge⁻ ($n = 3-16$) clusters

The structures of the found LLIs of In_{*n*}⁻, In_{*n*}Si⁻, and In_{*n*}Ge⁻ ($n = 3-16$) are displayed in Figure 1. The other three LLIs with slightly higher energy are shown in Figures S3-S5. Their optimized Cartesian coordinates at the BP86/def2-TZVP level are included in the Supporting information as well.

The calculations show that all small In_{*n*}⁻ ($n = 3-5$) clusters have plane structures. Starting from size 6, the three-dimensional structure begins to appear. The LLI of In₆⁻ has a triangular prism structure. For In₇⁻, the ground state structure can be derived from In₆⁻ by simply adding an extra In atom to one of the square faces. The calculations show that the LLI of In₈⁻ adopts a distorted cubic structure showing C_{2h} symmetry. This structure was previously predicted as the ground state for Al₈^{0,+1}, Ga₈, and In₈^{0,+1} clusters.^{10,21,25,28,29} For In₉⁻, a new ground-state structure has been obtained by adding one In atom on top of the In₈ cube. Previously, a ground state structure of In₉⁻ was reported by Shi et al.²⁸ which is identical as the isomer 9D with 0.164 eV higher energy as shown in Figure S3. The LLI of In₁₀⁻ can be obtained by adding two In atoms on top of In₈⁻ showing C_{2v} symmetry. This structure was also previously predicted as the favored one for the neutral, anionic, and cationic In₁₀ clusters.^{28,29} For In₁₁⁻, its lowest-lying structure can be regarded as forming by adding one In atom on the top and two more extra In atoms to the bottom of In₈⁻. It has been previously identified as the ground-state structure of the cationic, neutral, and anionic In₁₁.^{28,29} Moreover, neutral Al₁₁¹⁰ and Ga₁₁²⁵ also adopt the same configuration as their ground states. By capping one In atom on the neck of In₁₁⁻, it becomes the ground-state structure of In₁₂⁻. The energy of this structure is 0.028 eV lower than that of the lowest-energy structure previously reported²⁸ (see the 12B isomer in Figure S3). Our calculation shows that the icosahedral structure is not the favored one for In₁₃⁻ but with D_{5h} symmetry. For In₁₄⁻, the ground state structure can be derived from In₁₃⁻ by simply adding an extra In atom to one of the square faces. Both of the obtained lowest-lying structures of In₁₃⁻ and In₁₄⁻ agree with previous theoretical predictions.^{28,29} The LLIs of In₁₅⁻ and In₁₆⁻ have different structure pattern, showing prolate shapes. Here, the found In₁₅⁻ lowest-lying structure is 0.324 eV lower than the previously reported ground state²⁸ which is also found in this work as 15C isomer (it is can be seen in Figure S3). The LLI of the In₁₆⁻ cluster can be constructed by attaching an In atom on the waist of In₁₅⁻, which has been previously predicted to be the ground state of neutral In₁₆.²⁹

For Si and Ge atom doped Indium clusters, In_{*n*}Si⁻ and In_{*n*}Ge⁻ ($n = 3-16$), they all share the same structures except for $n = 8$. The structures of In_{*n*}Si⁻ and In_{*n*}Ge⁻ ($n = 3-4$) clusters have plane

FIGURE 1 Structures of LLI of In_n^- , In_nSi^- , and In_nGe^- ($n = 3-16$) clusters. For each structure, the symmetry is given on the left. Orange, green, and blue balls represent indium, silicon, and germanium atoms, respectively



structures. For size $n = 5$, they adopt quadrangular biconical structure with the semiconductor atom at the vertex site. The ground state structure of In_6X^- ($\text{X} = \text{Si}, \text{Ge}$) can be obtained by adding an X atom to one of the square faces of In_6^- . For the ground state structure of size $n = 7$, it can be constructed by adding an extra In atom to In_6X^- . For $n = 8$, the LLI of In_8Si^- can be seen as inserting a Si atom inside the In_8 cube, while In_8Ge^- adopts a boat-like structure as the structural motif with the Ge atom exposed on one side. The calculated energies show that this structure is 0.091 eV lower than that of cubic structure for In_8Ge^- . Both In_9Si^- and In_9Ge^- adopt the lowest-lying In_8Ge^- as the structural motif with an extra In atom attached on the neck. For In_nSi^- and In_nGe^- ($n = 10-12$), the lowest-lying structures for can be obtained by sequentially adding an In atom to its predecessor. It is worth noting that both $\text{In}_{12}\text{Si}^-$ and $\text{In}_{12}\text{Ge}^-$ adopt the same D_{5h} symmetric structure as In_{13}^- , indicating the dominance of geometric over the electronic order for this size. This structure was also predicted as the favored one for clusters In_{12}X and In_{12}X^- ($\text{X} = \text{Si}, \text{Ge}$, and Sn) previously.⁴⁷ For $n = 13$, the LLI of $\text{In}_{13}\text{Si}^-$ and $\text{In}_{13}\text{Ge}^-$ can be obtained by having five In atoms capping the five facets of the In_8Si^- and In_8Ge^- cubes, respectively. In the size range $n = 14-16$, for In_nSi^- and In_nGe^- , the lowest-energy structure for each cluster can also be obtained by adding an In atom to its predecessor. It worth to be noted that the $\text{In}_{14}\text{Si}^-$ and $\text{In}_{14}\text{Ge}^-$ can be obtained by replacing the encapsulated In atom of In_{15}^- with a Si or a Ge atom, respectively. It reflects the dominance of geometric order in these clusters which is the same as that happens in the case of $\text{In}_{12}\text{Si}^-$ and $\text{In}_{12}\text{Ge}^-$.

Structurally, the In_n^- clusters gradually grow to the D_{5h} symmetric In_{13} from $n = 3$, and the trend changes at size $n = 14$. For $n = 15$ and 16, they take completely different prolate type structures. Doping

one Si or Ge atom into an In_n^- cluster can significantly change its structure, except for sizes 3, 7, 8 and 10. The Si and Ge atoms are always surrounded by In atoms, and the In_nX^- ($\text{X} = \text{Si}, \text{Ge}$) clusters evolve into a closed D_{5h} symmetric structure ($n = 12$) starting from the structure of In_8X as a motif, and then continue to grow gradually taking In_{13}X as geometric basis.

3.2 | Structural determination

PES has been employed as fingerprints of clusters and molecules structures.^{19,48,49} Here, we compare the calculated PES with the experimental ones³³ to assess the correctness of the found lowest-lying structures in Figure 1 (Figures S6 and S7). All the measured spectra are reproduced fairly well by the calculated ones, which confirm the authenticities of predicted structures. It also shows the similarity of all the measured spectra of In_nSi^- and In_nGe^- for the same size except for $n = 8$, which reflects the likeness of the found structures for $n = 3-16$.

3.3 | Bonding and electronic properties of In_n^- , In_nSi^- , and In_nGe^- ($n = 8-16$)

Based on the found lowest-energy structures of the In_n^- , In_nSi^- , and In_nGe^- ($n = 3-16$), we further discuss their bonding and electronic properties by average bond lengths, Wiberg bond orders, VDE, HOMO-LUMO gaps, binding energies, and the second order differences in energy. The calculated results are presented in Figures 2 and 3 as well as summarized in Tables S2-S4.

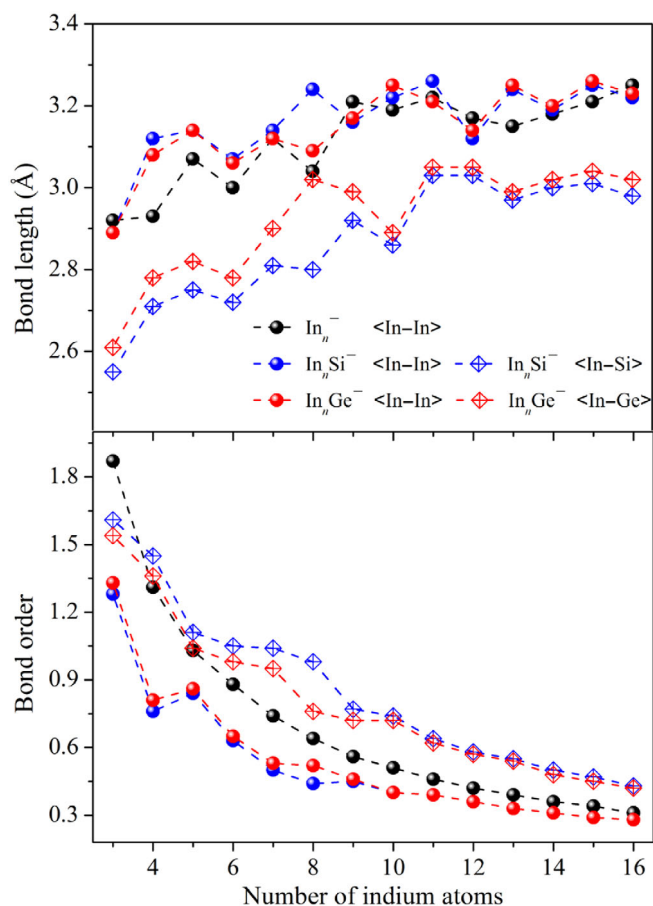


FIGURE 2 Average bond lengths and Wiberg bond orders of In–In, In–Si, and In–Ge of the ground-state structures of In_n^- , In_nSi^- , and In_nGe^- ($n = 3$ –16) clusters. The black, blue, and red balls represent the In–In bonds in In_n^- , In_nSi^- , and In_nGe^- , while the blue and red diamonds represent In–Si and In–Ge bonds, respectively

For pure In_n^- clusters, the lengths of In–In bonds show a gradually increasing trend which is consistent with their calculated bond orders. The average In–In bond lengths in In_{3-8}^- are significantly smaller (~ 0.1 Å) than that of larger clusters, and a slight even–odd oscillation appears in the size range of $n = 3$ –12. Doping one Si or Ge atom will extend the In–In bond in average for most sizes with a slight even–odd oscillation in the range $n = 11$ –16. The bond length of In–X ($X = \text{Si}, \text{Ge}$) is generally shorter than that of In–In bond. Both of bond length and bond order of In–Si and In–Ge are similar except for $n = 8$, again it shows the structure differences between In_8Si^- and In_8Ge^- . Also it is noticeable that the In–In bond lengths are insensitive to the dopant with size increase, however, the length of X–In ($X = \text{Si}$ and Ge) bond rather strongly correlates to the size of the dopant. Moreover, with size increase, the bond order of X–In ($X = \text{Si}$ and Ge) decreases linearly, which may indicate the existence of a turning point when the cluster larger than that, the X–In bond strength will not affect the formation of a jingle bell structure.

The VDEs (Figure 3A) of In_n^- , In_nSi^- , and In_nGe^- ($n = 3$ –16) show strong even–odd oscillations. Among In_n^- , In_{13}^- has the largest VDE which may indicate an electron closed shell formation according to shell model. The VDEs of all sized In_nSi^- and In_nGe^- ($n = 3$ –16) are very close, while, again the large difference between In_8Si^- and In_8Ge^- indicates their different structures.

The HOMO–LUMO gaps (Figure 3B) of all sized In_n^- , In_nSi^- , and In_nGe^- have the similar structures in the range of $n = 3$ –16, especially for In_nSi^- and In_nGe^- , which again indicates the insensitivity of the cluster configuration to the dopant. Moreover, the HOMO–LUMO gaps of In_n^- , In_nSi^- , and In_nGe^- ($n = 3$ –16) clusters show prominent even–odd oscillation, which can be attributed to the alternation of unpaired electron between even and odd sized clusters.

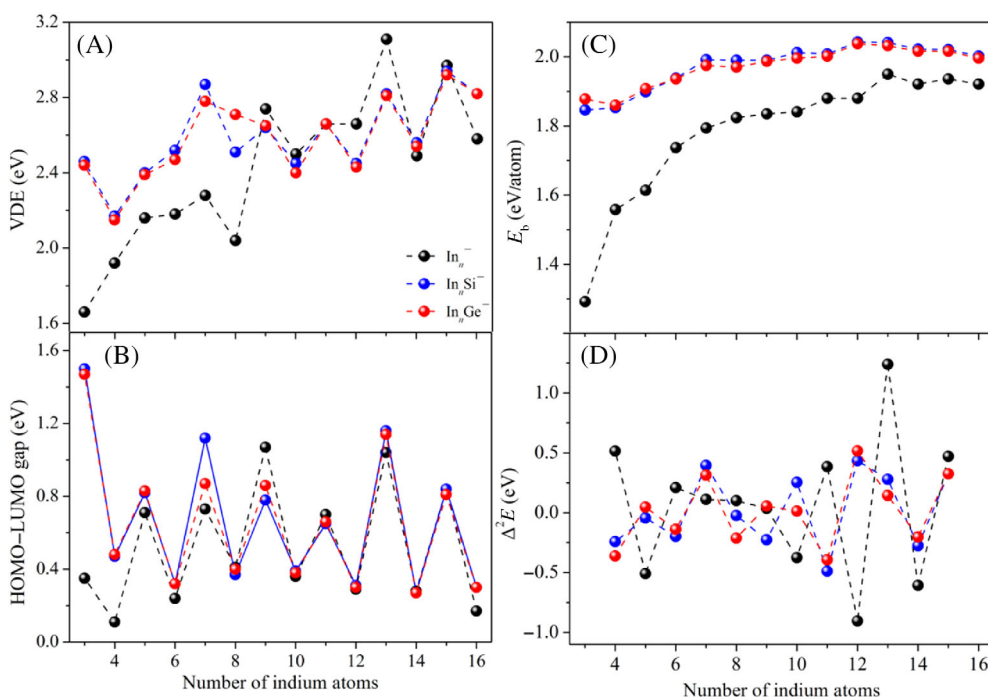


FIGURE 3 Size-dependent vertical detachment energy (VDE) (A), HOMO–LUMO gap (B), binding energies (E_b) (C), and second order differences in energy (Δ^2E) (D) of the ground-state structures of In_n^- , In_nSi^- , and In_nGe^- ($n = 3$ –16). The black, blue, and red balls represent In_n^- , In_nSi^- , and In_nGe^- , respectively

The binding energies (Figure 3C) of In_nSi^- and In_nGe^- are significantly higher than that of pure In_n^- clusters, signaling their enhanced stability due to the Si or Ge atom doping. The binding energy of In_nSi^- is very close to that of In_nGe^- in all sizes, hinting the similar effects of Si and Ge atoms doping to In_n^- clusters. Generally, the binding energy of both In_n^- and In_nX^- ($\text{X} = \text{Si}, \text{Ge}$) gradually increase and then decrease with a maximum at $n = 13$ and $n = 12$, respectively, which is associated to their perfect D_{5h} symmetry.

As shown in Figure 3D, the second order difference in energy (Δ^2E) of In_n^- also shows even-odd oscillation in size range $n = 9-15$, and the relative stability of odd sized clusters is higher than that of even sized clusters, which is related to the electron pairing. Again, the maxima of Δ^2E of pure In_n^- and In_nX^- ($\text{X} = \text{Si}, \text{Ge}$) appear at $n = 13$ and $n = 12$, respectively.

The above results show that In_nSi^- and In_nGe^- ($n = 3-16$) share very similar bonding and electronic properties except for size 8, which is the consequence of having the same geometric structures, therefore, the similar electronic configurations. Significantly, the In_{13}^- cluster not only has a perfect D_{5h} structure, but also has the largest VDE,

E_b and Δ^2E of all In_{3-16}^- clusters. Moreover, the In_{12}X^- ($\text{X} = \text{Si}, \text{Ge}$) with D_{5h} structure symmetric structure also owns the largest E_b and Δ^2E of all sizes.

3.4 | In_{13}^- , In_{12}Si , and In_{12}Ge as superatoms

As discussed above, the In_{13}^- has the largest VDE, E_b , and Δ^2E of all these pure In_n^- clusters, and In_{12}X^- ($\text{X} = \text{Si}, \text{Ge}$) has the same structure as In_{13}^- with one more electron than In_{13}^- , which prompts the study of In_{13}^- , and neutral In_{12}X ($\text{X} = \text{Si}, \text{Ge}$) as superatoms.⁵⁰⁻⁵² Therefore, we also examined the electronic structures neutral In_{12}X ($\text{X} = \text{Si}, \text{Ge}$). The D_{5h} symmetric structure is still for the lowest energy isomer of neutral In_{12}Si and In_{12}Ge .

The energy levels and spatial distributions of the occupied molecular orbitals of In_{13}^- , In_{12}Si , and In_{12}Ge clusters are illustrated in Figures 4 and 5.⁵³⁻⁵⁸ These three clusters behave as superatoms.⁵⁰⁻⁵² Interestingly, the electronic configurations of In_{13}^- and In_{12}X are $(1S)^2(1P)^6(1D)^{10}(2S)^2(1F)^{14}(2P)^6$ and $(1S)^2(1P)^6(2S)^2(1D)^{10}(1F)^{14}(2P)^6$,

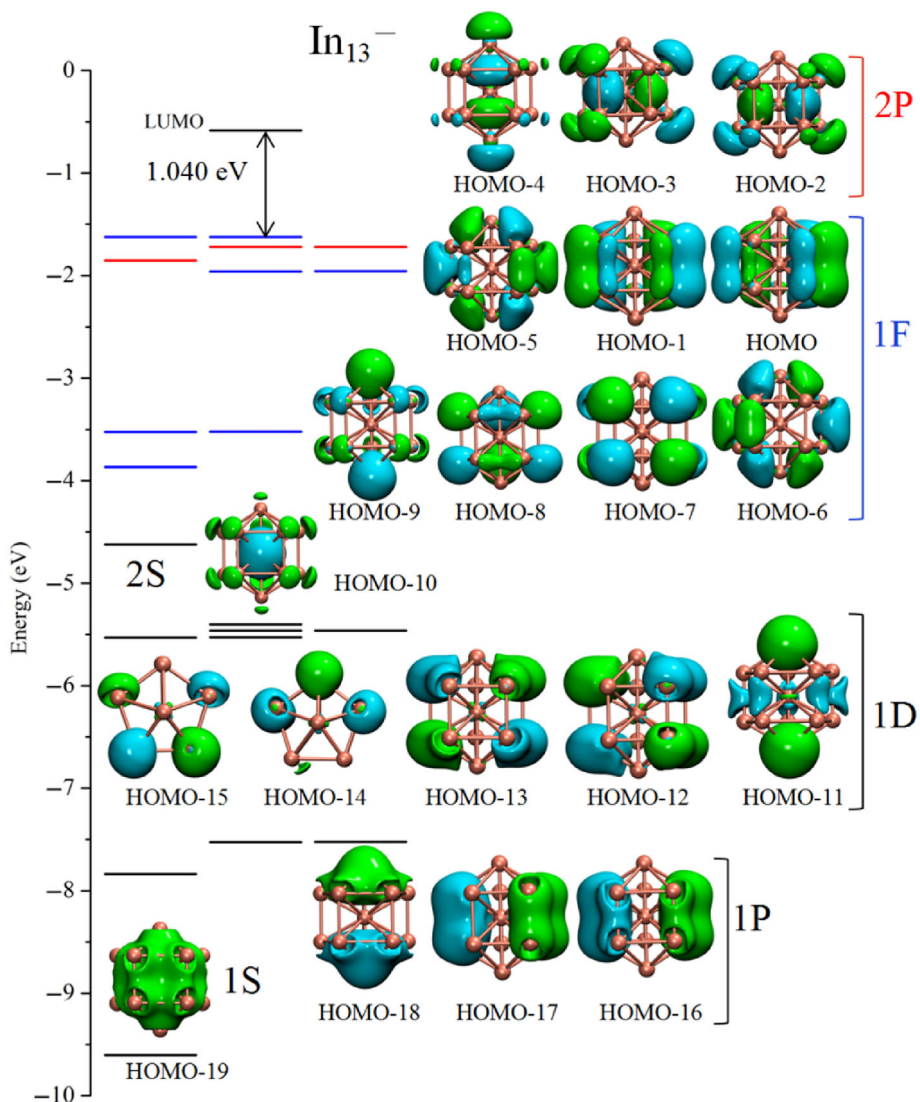


FIGURE 4 Energy levels and superatom orbitals for the In_{13}^- . The HOMO-LUMO gap is labeled on the corresponding level

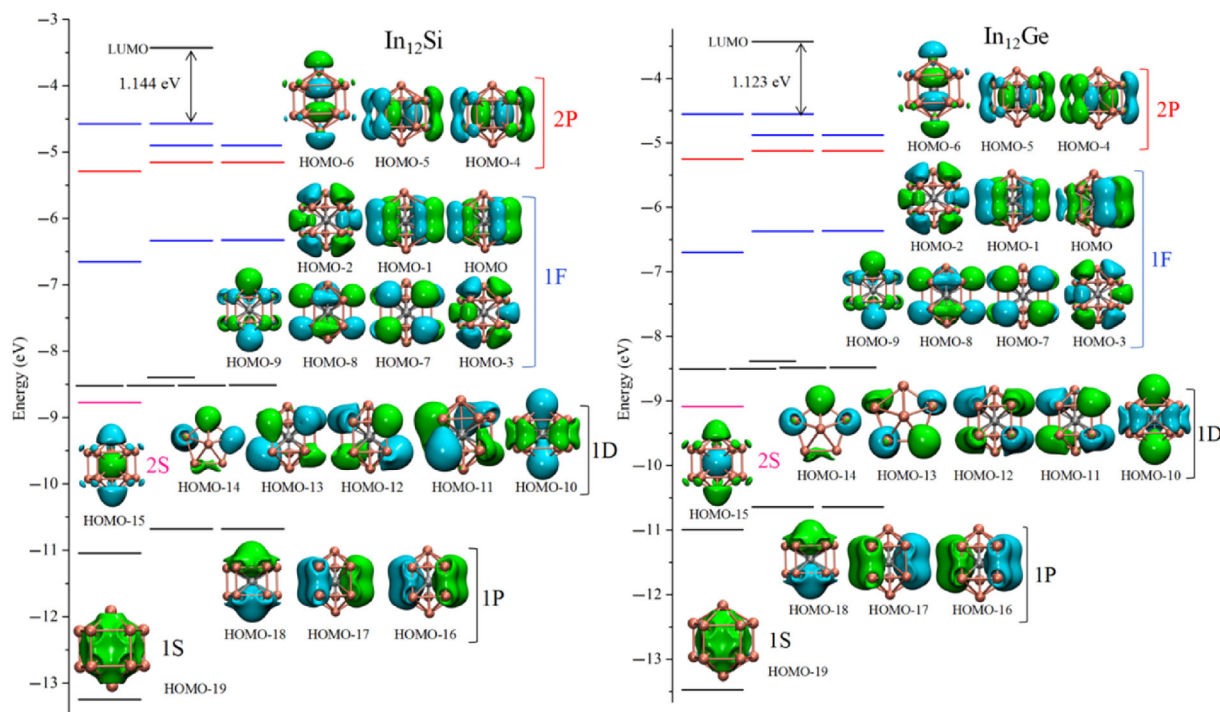


FIGURE 5 Energy levels and superatom orbitals for the neutral In_{12}Si and In_{12}Ge . The HOMO–LUMO gaps are labeled on the corresponding levels

respectively. The electronic configuration of In_{13}^- is consistent with the prediction of the shell model. The calculated HOMO–LUMO gaps of In_{12}Si and In_{12}Ge are 1.144 and 1.123 eV, respectively, both larger than that of In_{13}^- (1.040 eV), which suggest higher chemical stability. Moreover, In_{12}Si and In_{12}Ge have almost identical electronic configurations and spatial distributions of the occupied molecular orbitals, which again shows the similar doping effects of Si and Ge atoms to the indium clusters.

4 | CONCLUSIONS

The structural evolution and electronic properties of pure In_n^- and semiconductor atom-doped In clusters, In_nSi^- and In_nGe^- , were investigated through DFT calculations at BP86/def2-TZVP//BP86/def2-TZVPD level. For pure In_n^- , their structures evolve from planar (In_3) to cubic (In_8) to perfect D_{5h} symmetrical structure (In_{13}), and then changes the growth patten from spheroidal to prolate at $n = 15$. With one Si or Ge atom doping, the structures of the most sizes of In_n^- clusters change significantly with three types of motifs. Expect for $n = 8$, all of In_nSi^- and In_nGe^- clusters share very similar bonding and electronic properties in the size range of $n = 3$ –16 as a consequence of sharing the same geometric structures and therefore similar electronic configurations. The calculated average binding energies show that the dopant (Si or Ge) enhances the stability of In_n^- clusters. In_{13}^- and In_{12}X^- ($\text{X} = \text{Si}, \text{Ge}$) adopt highly symmetrical D_{5h} structure and having the largest E_b and Δ^2E in the size range of $n = 3$ –16. The In_{13}^- and neutral In_{12}X ($\text{X} = \text{Si}, \text{Ge}$) clusters are identified as superatoms

with electronic configurations of $(1\text{S})^2(1\text{P})^6(1\text{D})^{10}(2\text{S})^2(1\text{F})^{14}(2\text{P})^6$ and $(1\text{S})^2(1\text{P})^6(2\text{S})^2(1\text{D})^{10}(1\text{F})^{14}(2\text{P})^6$, respectively. These two doped clusters with closed electronic shells and high stability may be suitable as building blocks for assembling novel nanomaterials in future.

ACKNOWLEDGMENT

This work was supported by the National Natural Science Foundation of China (Grant No. 11774255), and the National Key R&D Program of China (No. 2020YFC2004602).

CONFLICT OF INTEREST

The authors declare no competing financial interest.

DATA AVAILABILITY STATEMENT

The authors confirm that the data supporting the findings of this study are available within the article and its supplementary materials.

ORCID

Lei Ma  <https://orcid.org/0000-0002-2446-4833>

REFERENCES

- [1] G. Ganteför, W. Eberhardt, *Chem. Phys. Lett.* **1994**, *217*, 600.
- [2] K. E. Schriver, J. L. Persson, E. C. Honea, R. L. Whetten, *Phys. Rev. Lett.* **1990**, *64*, 2539.
- [3] W. A. de Heer, P. Milani, A. Châtelain, *Phys. Rev. Lett.* **1989**, *63*, 2834.
- [4] C.-Y. Cha, G. Ganteför, W. Eberhardt, *J. Chem. Phys.* **1994**, *100*, 995.
- [5] J. Lermé, P. Dugourd, R. R. Hudgins, M. F. Jarrold, *Chem. Phys. Lett.* **1999**, *304*, 19.

- [6] K. J. Taylor, C. L. Pettiette, M. J. Craycraft, O. Chesnovsky, R. E. Smalley, *Chem. Phys. Lett.* **1988**, *152*, 347.
- [7] X. Li, H. Wu, X. B. Wang, L. S. Wang, *Phys. Rev. Lett.* **1909**, 1998, 81.
- [8] J. Akola, M. Manninen, H. Häkkinen, U. Landman, X. Li, L.-S. Wang, *Phys. Rev. B* **2000**, *62*, 13216.
- [9] R. O. Jones, *J. Chem. Phys.* **1993**, *99*, 1194.
- [10] B. K. Rao, P. Jena, *J. Chem. Phys.* **1890**, 1999, 111.
- [11] A. Aguado, J. M. López, *J. Chem. Phys.* **2009**, *130*, 064704.
- [12] W.-C. Lu, C. Z. Wang, L.-Z. Zhao, W. Zhang, W. Qin, K. M. Ho, *Phys. Chem. Chem. Phys.* **2010**, *12*, 8551.
- [13] Z. H. Li, A. W. Jasper, D. G. Truhlar, *J. Am. Chem. Soc.* **2007**, *129*, 14899.
- [14] A. K. Starace, C. M. Neal, B. Cao, M. F. Jarrold, A. Aguado, J. M. López, *J. Chem. Phys.* **2009**, *131*, 044307.
- [15] S. K. Nayak, S. N. Khanna, P. Jena, *Phys. Rev. B* **1998**, *57*, 3787.
- [16] Y. Ouyang, P. Wang, P. Xiang, H. Chen, Y. Du, *Comput. Theor. Chem.* **2012**, *984*, 68.
- [17] J. Zhao, L. Wang, J. Jia, X. Chen, X. Zhou, W. Lu, *Chem. Phys. Lett.* **2007**, *443*, 29.
- [18] X. Zhang, L. Guo, J. Guo, N. N. Ren, *Russ. J. Phys. Chem. A* **2014**, *88*, 457.
- [19] L. Ma, B. V. Issendorff, A. Aguado, *J. Chem. Phys.* **2010**, *132*, 104303.
- [20] Y. Zhao, W.-G. Xu, Q.-S. Li, Y.-M. Xie, H. F. Schaefer, *J. Phys. Chem. A* **2004**, *108*, 7448.
- [21] X. G. Gong, E. Tosatti, *Phys. Lett. A* **1992**, *166*, 369.
- [22] L. Guo, *Comp. Mater. Sci.* **2009**, *45*, 951.
- [23] S. Shi, Y. Liu, B. Deng, C. Zhang, G. Jiang, *Comp. Mater. Sci.* **2014**, *95*, 476.
- [24] C. Tang, S. Chen, W. Zhu, A. Zhang, K. Zhang, *Comput. Theor. Chem.* **2013**, *1014*, 8.
- [25] B. Song, P. L. Cao, *J. Chem. Phys.* **2005**, *123*, 144312.
- [26] S. Núñez, J. M. López, A. Aguado, *Nanoscale* **2012**, *4*, 6481.
- [27] L. Sai, J. Zhao, X. Huang, J. Wang, *J. Nanosci. Nanotechnol.* **2012**, *12*, 132.
- [28] S. Shi, Y. Liu, Y. Li, B. Deng, C. Zhang, G. Jiang, *Comput. Theor. Chem.* **2016**, *1079*, 47.
- [29] W. Q. Zhang, G. F. Zhao, J. M. Sun, L. L. Zhi, Y. Z. Gu, *Chem. Phys.* **2009**, *361*, 44.
- [30] W.-Q. Zhang, J. M. Sun, G.-F. Zhao, L.-L. Zhi, *J. Chem. Phys.* **2008**, *129*, 064310.
- [31] W. Q. Zhang, T. G. Liu, Y. Z. Bai, *Comput. Theor. Chem.* **2012**, *986*, 57.
- [32] R. C. Longo, J. Carrete, F. Aguilera-Granja, A. Vega, L. J. Gallego, *J. Chem. Phys.* **2009**, *131*, 074504.
- [33] M. Akutsu, K. Koyasu, J. Atobe, K. Miyajima, M. Mitsui, A. Nakajima, *J. Phys. Chem. A* **2007**, *111*, 573.
- [34] K. Wang, Z.-Z. Jia, Z. Fan, H.-Y. Zhao, G.-J. Yin, R. Moro, B. V. Issendorff, L. Ma, *Phys. Chem. Chem. Phys.* **2022**, *24*, 8839.
- [35] K. Wang, H.-Y. Zhao, L. Miao, Z.-Z. Jia, G.-J. Yin, X.-D. Zhu, R. Moro, B. V. Issendorff, L. Ma, *J. Phys. Chem. A* **2022**, *126*, 1329.
- [36] K. Wang, G.-J. Yin, Z.-Z. Jia, L. Miao, R. Moro, B. V. Issendorff, L. Ma, *Phys. Chem. Chem. Phys.* **2022**, *24*, 18321.
- [37] F. Neese, F. Wennmohs, U. Becker, C. Riplinger, *J. Chem. Phys.* **2020**, *152*, 224108.
- [38] F. Weigend, R. Ahlrichs, *Phys. Chem. Chem. Phys.* **2005**, *7*, 3297.
- [39] F. Weigend, *Phys. Chem. Chem. Phys.* **2006**, *8*, 1057.
- [40] A. D. Becke, *Phys. Rev. A* **1988**, *38*, 3098.
- [41] J. P. Perdew, *Phys. Rev. B* **1986**, *33*, 8822.
- [42] D. Rappoport, F. Furche, *J. Chem. Phys.* **2010**, *133*, 134105.
- [43] F. Neese, *J. Comput. Chem.* **2003**, *24*, 1740.
- [44] J. Akola, M. Manninen, H. Häkkinen, U. Landman, X. Li, L.-S. Wang, *Phys. Rev. B* **1999**, *60*, R11297.
- [45] W. Humphrey, A. Dalke, K. Schulten, *J. Mol. Graph.* **1996**, *14*, 33.
- [46] T. Lu, F. Chen, *J. Comput. Chem.* **2012**, *33*, 580.
- [47] Y. Liu, K. Deng, Y. Yuan, X. Chen, H. Wu, X. Wang, *Chem. Phys. Lett.* **2009**, *469*, 321.
- [48] O. Kostko, B. Huber, M. Moseler, B. V. Issendorff, *Phys. Rev. Lett.* **2007**, *98*, 043401.
- [49] A. Aguado, A. Vega, A. Lebon, B. V. Issendorff, *Nanoscale* **2018**, *10*, 19162.
- [50] A. W. Castleman Jr., S. N. Khanna, *J. Phys. Chem. C* **2009**, *113*, 2664.
- [51] Z. Luo, A. W. Castleman, *Acc. Chem. Res.* **2014**, *47*, 2931.
- [52] P. Jena, *J. Phys. Chem. Lett.* **2013**, *4*, 1432.
- [53] F. Bruneval, N. Vast, L. Reining, *Phys. Rev. B* **2006**, *74*, 045102.
- [54] R. Stowasser, R. Hoffmann, *J. Am. Chem. Soc.* **1999**, *121*(14), 3414.
- [55] R. V. Meer, O. V. Gritsenko, E. J. Baerends, *J. Chem. Theory Comput.* **2014**, *10*(10), 4432.
- [56] R. Laplaza, C. Cárdenas, P. Chaquin, J. Contreras-García, P. W. Ayers, *J. Comput. Chem.* **2021**, *42*, 334.
- [57] E. J. Baerends, *J. Chem. Phys.* **2018**, *149*, 054105.
- [58] E. J. Baerends, O. V. Gritsenko, R. V. Meerab, *Phys. Chem. Chem. Phys.* **2013**, *15*, 16408.

SUPPORTING INFORMATION

Additional supporting information can be found online in the Supporting Information section at the end of this article.

How to cite this article: K. Wang, L. Miao, Z. Jia, R. Wang, G. Yin, X. Zhu, R. Moro, L. Ma, *J. Comput. Chem.* **2022**, *1*. <https://doi.org/10.1002/jcc.26998>